Journal of Petroleum Science and Engineering 210 (2022) 109956

Contents lists available at ScienceDirect

Journal of Petroleum Science and Engineering

journal homepage: www.elsevier.com/locate/petrol

An improved rock typing method for tight sandstone based on new rock typing indexes and the weighted fuzzy kNN algorithm

Lili Ji [a], Mian Lin [a,b,*], Wenbin Jiang [a,**], Gaohui Cao [a], Zhipeng Xu [a], Fang Hao [c]

[a] Key Laboratory for Mechanics in Fluid Solid Coupling Systems, Institute of Mechanics, Chinese Academy of Sciences, Beijing, 100190, China
[b] School of Engineering Science, University of Chinese Academy of Sciences, Beijing, 100190, China
[c] School of Geosciences, China University of Petroleum, Shandong, 266555, China

ARTICLE INFO

Keywords:
New rock typing indexes
The weighted fuzzy kNN algorithm
Tight sandstone
Non-Darcy flow

ABSTRACT

Petrophysical rock typing is a very important problem in flow unit interpretation and reservoir characterization. Unlike the sandstone, the presence of numerous nanopores in tight sandstone can cause strong gas and liquid non-linear flow. And this makes the traditional rock typing indexes derived from Darcy'law unsuitable for tight sandstone. In this paper, new rock typing indexes, including the Darcy index (Fi), the gas non-Darcy index (Kc) and the liquid non-Darcy index (Sr), have been proposed to describe the non-linear flow characteristics in tight sandstone. In addition, the limit pore ranges for gas and liquid non-Darcy flow have been determined based on these indexes. Then the weighted fuzzy kNN algorithm, which can consider the weight differences between different rock typing indexes, is combined with three indexes to improve the accuracy of rock typing. In order to test the rock typing indexes and the weighted fuzzy kNN algorithm, the tight sandstone dataset in Upper Triassic Yanchang Formation, Ordos Basin, NW China has been constructed with RES (representative element surface) random pore network and experiment data. The results show that the new rock typing indexes and the weighted fuzzy kNN algorithm have better performance in typing tight sandstone than the traditional methods. Moreover, 30 mercury injection capillary pressure (MICP) curves measured on highly inhomogeneous tight sandstone samples from the research area have also been used to validate our method. All the results have proved that the proposed new rock typing indexes and weighted fuzzy kNN algorithm can type the tight sandstone very well, and they play a significant role in permeability prediction, reservoir modeling and simulation.

1. Introduction

Petrophysical rock typing, generally grouping rocks according to a similar property, is widely used in identifying fluid units, predicting permeability and capillary pressure curves in flow units, and modeling the reservoirs(Abbaszadeh et al., 1996; Oliveira et al., 2016; Chen and Yao, 2017; Roque et al., 2017; Saboorian-Jooybari, 2017; Rafiei and Motie, 2019). However, most traditional rock typing methods are only applicable to homogeneous sandstone in the conventional reservoir. When used to analyze the tight sandstone with multiscale pore structure and multiple fluid flow mechanisms in unconventional reservoirs, they do not work very well. Therefore, it is necessary to develop a new rock typing method to characterize the tight sandstones.

In the past decades, many efforts have been made in rock classification. Generally, the petrophysical rock typing methods can be roughly divided into two categories, petrophysical static rock typing and petrophysical dynamic rock typing. The petrophysical static rock typing method mainly classifies rocks according to capillary pressure data. Some studies have shown that the r35, the pore-throat radius at the 35th percentile mercury saturation, can reflect the deposition and the fluid flow of the rock (Hartmann and Coalson, 1990). Then Martin et al. (1997) have divided the reservoir into four different fluid units based on r35. However, in actual reservoirs, it is usually very difficult to use one pore-throat size to characterize the fluid flow of rocks. Later, the dimensionless function of water saturation called the J(s)-function was proposed to calculate the capillary pressure curves and classify the pore structure of rocks (Leverett, 1941; Stolz and Graves, 2003). Although the J(s)-function provides a practical approach to typing rocks, it can only

* Corresponding author. Key Laboratory for Mechanics in Fluid Solid Coupling Systems, Institute of Mechanics, Chinese Academy of Sciences, Beijing, 100190, China.
** Corresponding author.
E-mail addresses: linmian@imech.ac.cn (M. Lin), jiangwenbin@imech.ac.cn (W. Jiang).

https://doi.org/10.1016/j.petrol.2021.109956
Received 18 September 2021; Received in revised form 26 November 2021; Accepted 29 November 2021
Available online 3 December 2021

be used for grouping cores with similar geometries (Stolz and Graves, 2003). In addition, the capillary pressure experimental measurement for lots of rocks in the reservoir is costly, which also makes the petrophysical static rock typing method difficult to be widely used.

The petrophysical dynamic rock method mainly classifies rocks based on permeability and porosity. The pioneering work in this area lies in Berg (1970), who proposed that the permeability and porosity of rocks may be related to the composition, texture and pore size of the rock. Lucia (1983) has investigated the characteristics of carbonate rocks and found that there was a good correlation among permeability, porosity and grain size. By analyzing some carbonate and sandstone rock samples, the widely used Winland equation, which linked the permeability and porosity to the pore-throat size, has been proposed (Kolodzie, 1980). Then numerous empirical models have been proposed to establish a correlation between the permeability, porosity and a characteristic pore-throat size corresponding to different mercury injection saturations (Pittman, 1992; Jaya et al., 2005; Rezaee et al., 2012; Ngo et al., 2015). However, the performance of these empirical models largely depends on the quality of data used for developing them and optimizing the fitting parameters. At the same time, other researchers have developed new theoretical indexes for rock typing based on the Kozeny-Carman equation (Amaefule et al., 1993; Nooruddin and Hossain, 2011; Ferreira et al., 2015). Likewise, Amaefule et al. (1993) have used the modified Kozeny-Carman equation to derive the flow-zone indicator (FZI). Recently, Mirzaei-Paiaman et al. (2018) have developed a new index (FZI-Star) based on the Kozeny-Carman equation and Darcy'law. However, when these indexes are used to model the fluid units in tight sandstone reservoirs, their performance is not very good. This is because the Kozeny-Carman equation is derived from Hagen-Poissoulle's and Darcy's law, and it cannot describe the non-Darcy flow in porous media. While the tight sandstone has numerous nanopores which can cause strong non-Darcy flow. Thus it is necessary to develop new rock typing indexes suitable for the tight sandstone.

In this paper, new rock typing indexes are proposed, and then they are combined with the data mining method to type the tight sandstone. The paper is arranged as follows. First, the Darcy flow, the gas non-Darcy flow and the liquid non-Darcy flow of tight sandstone are analyzed. The rock typing indexes proposed in this paper are described in detail. The limit pore radiuses for gas and liquid non-Darcy effect are investigated. Second, a weighted Fuzzy k-Nearest Neighbor (kNN) algorithm is presented to take into account the weight difference between different indexes. Third, the tight sandstone dataset and some experimental results are used to validate the rock typing method proposed in this paper. Finally, some important results are summarized.

2. Methodology

2.1. The new rock typing indexes for typing tight sandstones

It is well known that the petrophysical rock typing index should represent the fluid flow characteristics in the rock. Furthermore, note that the pore network of the rock can greatly influence fluid flow, thus the petrophysical rock typing index should also represent the characteristics of the pore network including: the pore size and shape, the throat size and shape, the pore-throat ratio and the connectivity of the pores.

To derive the new rock typing indexes, we first investigate the characteristics of the pore space and fluid flow mechanism in tight sandstone. Fig. 1 shows the typical pore-throat size distribution of conventional sandstone and tight sandstone (Li et al., 2021; Xu et al., 2021). It can be seen that the pore space of tight sandstone with multiscale structure is much more heterogeneous than that of the conventional sandstone. As a result, the MICP curve of tight sandstone is much more complicated than that of conventional sandstone (Fig. 2). Thus we can easily obtain that the traditional index (r35 and the mean pore size) cannot fully describe the characteristics of the multiscale pore space in tight sandstone. Moreover, because of the non-Darcy fluid flow in nanopores of tight sandstone, the experiment measured permeability of tight sandstone changes with pressure, as shown in Fig. 3. While the permeability of conventional sandstone does not change with pressure. Thus the traditional index FZI, which is derived from Darcy law, cannot fully describe the fluid flow characteristics in tight sandstone (see Fig. 3).

In this paper, three new indexes, including the Darcy index (Fi), the gas non-Darcy index (Kc) and the liquid non-darcy index (Sr), are introduced to represent the fluid flow characteristics in the multiscale pore structure in tight sandstone. In the following, these indexes will be described in detail.

2.1.1. The Darcy index (Fi)

First, the Darcy permeability is used to derive the Darcy index. Unlike the Kozeny-Carman equation that has been used extensively in the conventional reservoir, the Darcy permeability equation proposed by Jiang (Jiang et al., 2017) is used in our study.

$$Kd = \frac{\varphi_f R_{nt}^2}{8\tau} \tag{1}$$

$$R_{nt} = \left(\frac{1}{N} \sum_{i=1}^{N} \left(\frac{1}{r_i} \right)^{D_f - 3} \right)^{-\frac{1}{D_f - 3}} \tag{2}$$

Where Kd is the Darcy permeability, r_i, N, φ_f are the$i$th pore radius, the total number of pores and the flowing porosity. $\tau$is the tortuosity of the rock. D_f is the fractal dimension of the pore surface, and it is introduced to consider the effect of pore-surface roughness on the Knudsen diffusion coefficient (Coppens, 1999; Coppens and Dammers, 2006; Jiang et al., 2017).

In this equation, the term $\frac{R_{nt}^2}{8\tau}$describes some microscopic properties, which include the pore size, the pore information and the tortuosity of the pore network. Note that if$D_f = 2$, R_{nt} is equal to the mean pore

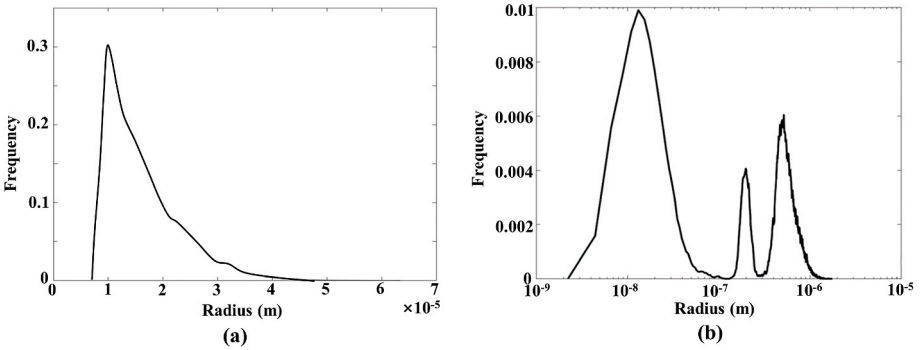

Fig. 1. The pore-throat distribution of conventional sandstone (a) and tight sandstone (b).

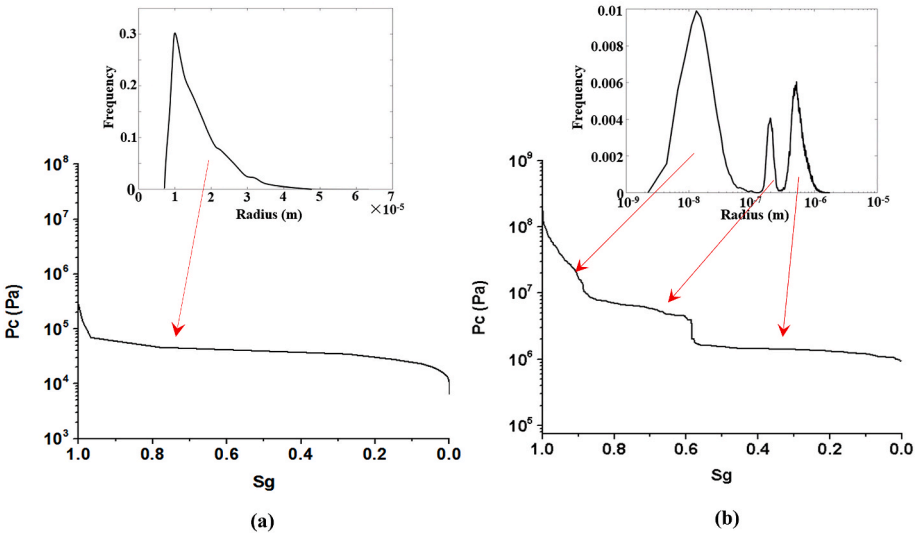

Fig. 2. The MICP curve of conventional sandstone (a) and tight sandstone (b).

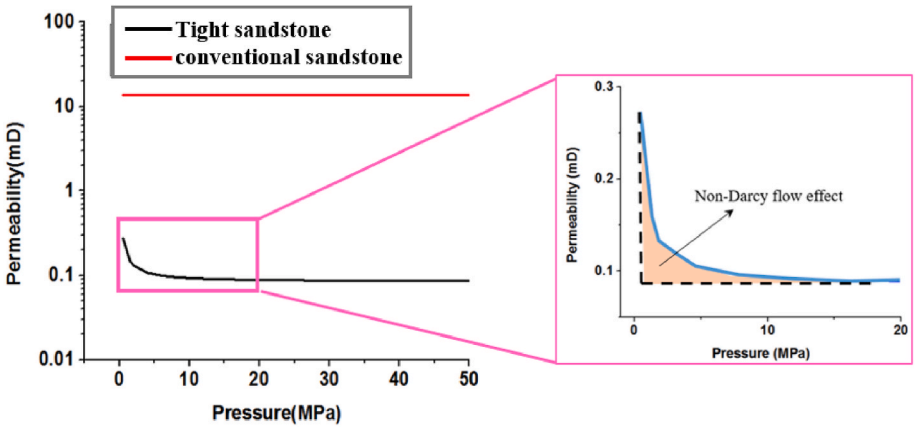

Fig. 3. The apparent permeability of conventional sandstone and tight sandstone.

radius of the tight sandstone. Thus in this study $\frac{R_{nt}^2}{8\tau}$ is used as one of the flow zone indicators, and denoted as Fi. The equation of Fi can be written as

$$Fi = \sqrt{\frac{Kd}{\varphi}} = \frac{R_{nt}}{\sqrt{8\tau}} \tag{3}$$

Then we compare Fi with the traditional index FZI. The index FZI can be calculated by the following formula

$$FZI = \frac{1}{\sqrt{F_s}\tau S_{gv}} \tag{4}$$

where F_s, τ and S_{gv} are the shape factor of capillary tubes, the tortuosity and the surface area per unit grain volume. It is obvious that FZI is a function of the tortuosity, shape factor and grain diameter, while Fi is a function of the tortuosity and R_{nt}. Note that the key influencing factors of the fluid flow in rocks are not the property of the matrix component (grain diameter) but rather the property of pores and throats. The R_{nt} in Fi contains the information of the pore and throat in tight sandstone. Thus Fi is more suitable for typing tight sandstone than FZI.

In fact, Darcy permeability is the absolute permeability, and it is an inherent property of the rock and independent of pressure.

2.1.2. The gas non-Darcy index (Kc)

As mentioned above, the tight sandstone has a multiscale pore structure, and especially contains numerous nanopores. Nanopores cause non-Darcy flow in tight sandstone.

To describe the gas non-Darcy flow in tight sandstone, Jiang (Jiang et al., 2017) has proposed the apparent permeability (AP) formula for tight sandstone accounting for slip flow and Knudsen diffusion. The formula can be written as

$$\begin{cases} Kapp_{gas} = \dfrac{2R_{nt}\mu\varphi_f}{3\rho_{avg}\tau}\left(\dfrac{d_m}{2R_{nt}}\right)^{D_f-2}\sqrt{\dfrac{8M}{10^3\pi RT}} + Kd \times \left(1 + \sqrt{\dfrac{8\cdot 10^3\pi RT}{M}}\ \dfrac{\mu}{R_{avg}p_{avg}}\left(\dfrac{2}{\alpha} - 1\right)\right) \\ R_{avg} = \left(\dfrac{1}{N}\sum_{i=1}^{N}\dfrac{1}{r_i}\right)^{-1} \end{cases} \tag{5}$$

where $Kapp_{gas}$ is the apparent permeability for gas. M, μ refer to the molar mass and the viscosity of the gas, respectively. p_{avg} is the pressure. T refers to the experimental temperature, and R is the gas constant. Moreover, the term $\frac{2R_{nt}\mu\varphi_f}{3\rho_{avg}\tau}\left(\frac{d_m}{2R_{nt}}\right)^{D_f-2}\sqrt{\frac{8M}{10^3\pi RT}}$ describes the Knudsen diffusion, and the term $Kd\times\sqrt{\frac{8\cdot10^3\pi RT}{M}}\ \frac{\mu}{R_{avg}p_{avg}}\left(\frac{2}{\alpha}-1\right)$ describes the slip flow.

According to the above equation, the terms $\frac{2R_{nt}\mu\varphi_f}{3\rho_{avg}\tau}\left(\frac{d_m}{2R_{nt}}\right)^{D_f-2}\sqrt{\frac{8M}{\pi RT}}$ and $\sqrt{\frac{8\pi RT}{M}}\ \frac{\mu}{R_{avg}p_{avg}}\left(\frac{2}{\alpha}-1\right)$ contain non-Darcy flow properties induced by the nanopores of the tight sandstone. Therefore, the non-Darcy index is derived as below

$$Kc=\frac{\mathrm{Kapp}_{gas}}{\mathrm{Kd}}-1 \tag{6}$$

Where Kc refers to the gas non-Darcy index.

The gas non-Darcy index in Eq. (5) not only includes the gas flow properties in the rock, but also reflects some microstructure information of the rock properties. Considering the pore network with numerous pores is complex and not suitable for mechanism research, we choose one pore to investigate the change rule of Kc and determine the limit values of the main controlling factors. It should be pointed out that under this condition Eq. (2) can be simplified to Rnt = r. Fig. 4 plots the variety of Kc with the surface fractal dimension Df and the pore size for different pressure. It can be seen that Kc decreases as Df, pore radius and pressure increase. Considering that Kd increases with the pore size and Kc decreases with the pore size, we can deduce that Kc can reflect the characteristic of small pores in the rock.

According to the above analysis, we know that Kc decreases gradually with the increase of the pore radius. Thus we can further determine the limit pore radius that needs to consider the gas non-Darcy flow based on equations (5) and (6). It is assumed that when Kc is less than 20%, the gas non-Darcy effect can be ignored, and the corresponding pore radius is defined as the gas non-Darcy limit pore size (denoted by R_{Kc}). Considering that the gas non-Darcy effect includes the Knudsen effect and slip effect, we will discuss them separately here. Similar to Kc, the index for Knudsen effect in gas non-Darcy effect is assumed to be Knr, and it can be calculated as follows

$$Knr=\frac{\frac{2R_{nt}\mu\varphi_f}{3\rho_{avg}\tau}\left(\frac{d_m}{2R_{nt}}\right)^{D_f-2}\sqrt{\frac{8M}{10^3\pi RT}}}{\mathrm{Kd}} \tag{7}$$

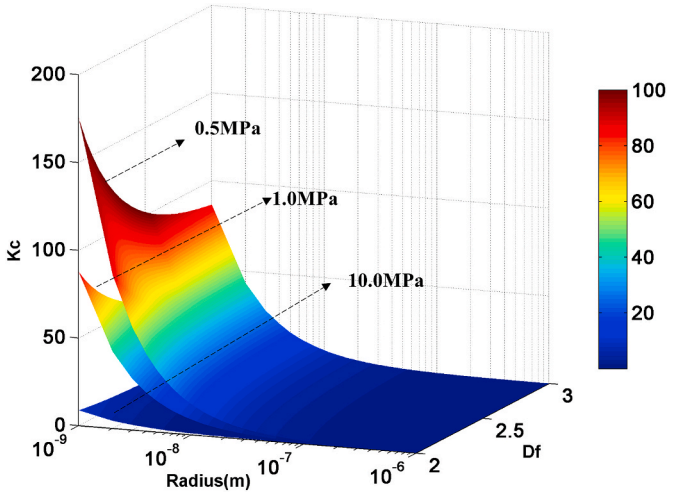

Fig. 4. The gas non-Darcy index Kc for different pressure.

Similarly, it is also assumed that when Knr is less than 20%, the Knudsen effect in tight sandstone can be ignored, and the corresponding pore radius is Knudsen effect limit pore radius, denoted by R_{Knr}. Next, we determine the value of R_{Kc}和R_{Knr}. According to Eqs. (5)–(7), Knr and Kc are related to the surface fractal dimension Df, the pressure and the pore radius. Based on the analysis of the actual tight sandstone samples, we know that the surface fractal dimension varies from 2 to 3, and most of them are bigger than 2.5 (Jiang et al., 2017). Therefore, we will discuss the limit pore radius when Df is 3. We investigate the variation law of Knr and Kc with pore radius and pressure when Df is 3, as shown in Fig. 5. It can be seen that Knr and Kc decrease rapidly with the increase of pressure and pore size. Considering that in the actual production of tight sandstone gas, the minimum wellhead pressure is 0.5 MPa. If pressure is less than 0.5 MPa, the production of tight gas will stop (Li et al., 2019). Therefore, when the values of Knr and Kc are 0.2 at 0.5 MPa, the corresponding pore radiuses are the limit pore radiuses. We then obtain from Fig. 5 that R_{Kc} and R_{Knr} are 450 nm and 20 nm, respectively. When the pore radius is greater than 20 nm, Knudsen diffusion of the gas disappears. When the pore radius is greater than 450 nm, the gas slip effect can be ignored. At this time, only Darcy flow needs to be considered, as shown in Fig. 6.

Further, we can deduce from the above discussion that when the rock sample contains more pores smaller than R_{Kc}, the value of Kc becomes larger. Kc can indirectly reflect the information of the small pores (less than R_{Kc}).

2.1.3. The liquid non-Darcy index (Sr)

Eq. (5) is the apparent permeability of the gas in tight sandstone. Typing the tight sandstone should also consider the liquid flow. Unlike the liquid flow in sandstone, there are slip flow effect in the nanopores of tight sandstone, which should be considered during typing the rocks. Afsharpoor and Javadpour (2016) has proposed a closed-form generalized fluid-flow equation

$$Q=\frac{A^2}{\mu L}\left[a+bL_{sd}+cG+dL_{sd}^2+eG^2+fL_{sd}G\right]\triangle p \tag{8}$$

$$G=\frac{A}{CL_c},\quad L_{sd}=\frac{L_s}{\sqrt{A}} \tag{9}$$

where coefficients a–f are empirical constants as listed in Table 1, Q is volumetric flow rate, A is cross-sectional area, L is duct length, and $\triangle p$ is pressure drop. C is perimeter, Lc is characteristic length (Lc is perimeter [C] in a straight single duct), $\mu$is viscosity, and Ls is slip length.$L_{sd}$is dimensionless slip length, and G is dimensionless shape factor.

Based on Eq. (8), we can calculate the liquid apparent permeability of the tight sandstone. Similar to the definition of the gas non-Darcy effect index Kc, the liquid non-Darcy index is defined as Sr. Its expression is as follows

$$Sr=\frac{Kapp_{liquid}}{Kd}-1 \tag{10}$$

Where$Kapp_{liquid}$is the liquid apparent permeability,and Srrefers to the liquid non-Darcy index.

Next, we examine the influencing factors and changing laws of the liquid non-Darcy index Sr. It can be obtained from Eq. (8) that Sr is mainly related to the shape factor, slip length and pore radius. A lot of experimental studies have shown that the slip length of water should generally be less than 20 nm (Audry et al., 2010; Cottin et al., 2005). Here we assume that the slip length is 20 nm to discuss the problem. Then the variation of Sr with pore radius and shape factor is shown in Fig. 7. It can be seen that for each shape factor, Sr decreases rapidly with the increase of the pore radius. While for each pore radius, Sr first decreases and then increases with the shape factor. Similar to the discussion of gas in the previous section, we also assume that when Sr is less

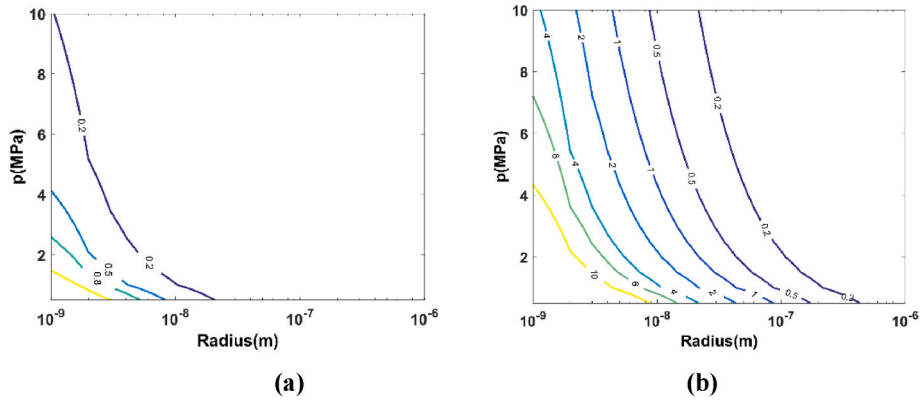

Fig. 5. The contour map for Knr (a) and Kc(b).

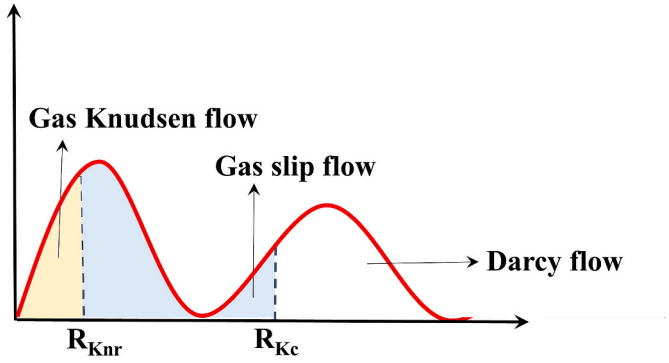

Fig. 6. The sketch of R_{Knr} and R_{Kc} (If the pore radius is smaller than $R_{Kc,}$ there is gas non-Darcy flow in it).

Table 1
Coefficients a–f in the closed-form generalized fluid-flow equation.

	a	b	c	d	e	f
G≥ 0.04	−0.16	0.12	6.4	−5.5E-03	−50.0	1.7
G < 0.04	−1.2E-02	5.7E-02	2	−5.2E-03	−38.0	3.2

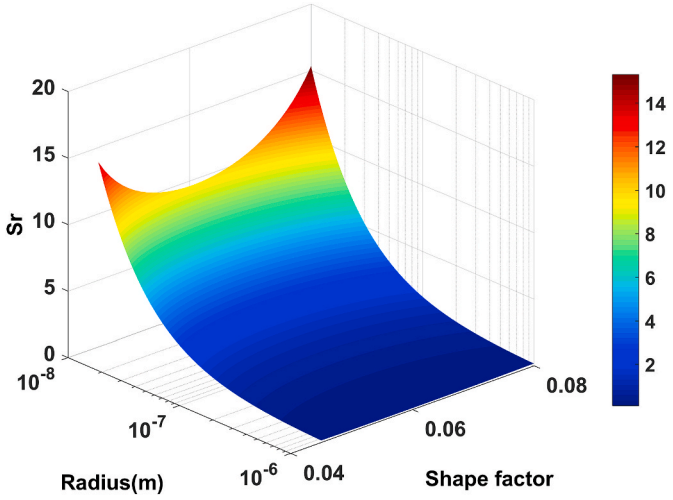

Fig. 7. The liquid non-Darcy index Sr vs the pore radius and shape factor.

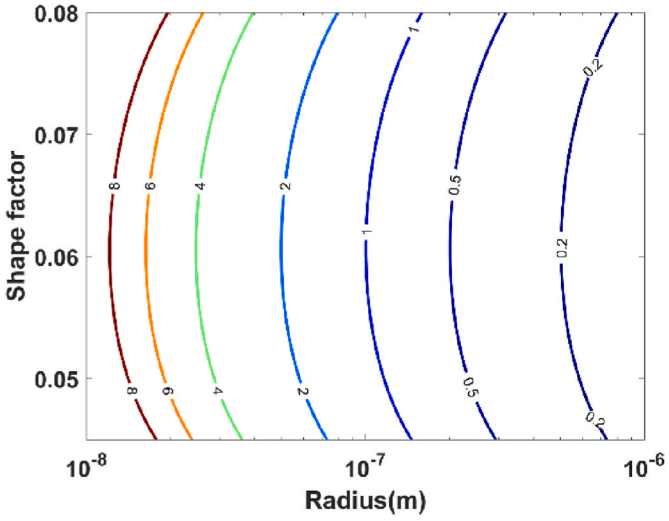

Fig. 8. The contour map for Sr.

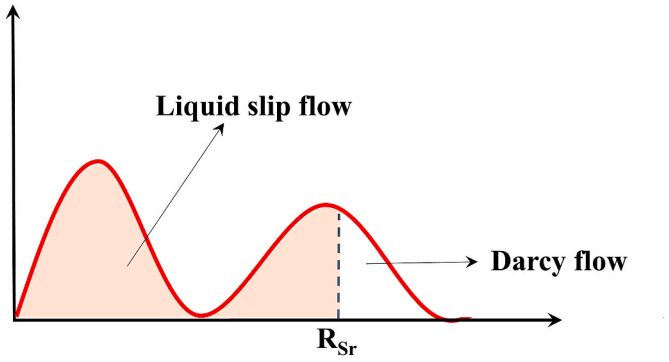

Fig. 9. The sketch of R_{Sr} (If the pore radius is smaller than $R_{Sr,}$ there is liquid non-Darcy flow).

than 20%, the liquid non-Darcy effect can be ignored, and the corresponding pore size is the limit pore radius, expressed by R_{Sr}. To get the value of R_{Sr}, Fig. 8 shows the contour map of Sr. It can be seen that when the shape factor is 0.08 (circular pore), the limiting radius R_{Sr} can be obtained as 800 nm. That is, when the pore radius is greater than 800 nm, the liquid non-Darcy effect can be ignored, as shown in Fig. 9. Further, we can also infer that when the rock sample contains more pores smaller than R_{Sr}, the value of Sr becomes larger. Sr reflects the information of the small pores (less than R_{Sr}).

Finally, according to the gas non-Darcy limit pore size and liquid non-Darcy limit pore size, we can divide the pores into three parts: the first part is the pores with a radius smaller than R_{Kc}, the second part is the pores with a radius greater than R_{Kc} and less than R_{Sr}, and the third part is the pores with a radius greater than R_{Sr}. Obviouly there will be gas non-Darcy flow and liquid non-Darcy flow in the first part of the pores, and thus we name this part of pores as P_G. There is only liquid non-Darcy effect in the second part of the pores, the gas non-Darcy flow disappears, and thus we name it as P_L. There is only Darcy flows in the third part of the pores, and we name it as P_D. The value of Kc, Sr and Kd can indirectly reflect the proportions of three types of pores in the rock sample.

From all the above discussion, we can obtain that the three new rock typing indexes proposed in this paper can represent the complex flow characteristics (Darcy flow, gas non-Darcy flow, the liquid slip flow) and some information of the pore structure. In the follwing secton, we will discuss how to use them to type tight sandstone.

2.2. Typing rocks based on the proposed indexes and the weighted fuzzy kNN algorithm

Through the analysis of the indexes in the previous section, we can deduce that the three newly proposed indexes play different roles in typing tight sandstone. Thus during typing rocks, these indexes should not be assigned the same weight. In the following, we will describe the calculation process of the weights for the three indexes in detail.

As is well known, the k-nearest neighbor algorithm (kNN) is one of the oldest and simplest non-parametric pattern classification methods. In the KNN algorithm, the classes are assigned according to the most common class amongst its k-nearest neighbors. However, the KNN algorithm does not consider the relative relationship between sample features. The classification speed is slow and the calculation complexity is high. Unlike the standard k-Nearest Neighbor classifier, the fuzzy k-Nearest Neighbor (kNN) classifier uses a fuzzy membership function to weight the k nearest neighbors based on the distances between the query points. Although the fuzzy kNN improves the performance of kNN, other data-related parameters need to be optimized. In addition, the fuzzy kNN does not consider the influence of the representative characteristics of the data points, which may be noisy, redundant, and may not contain useful information to clearly identify a specific class. The weighted fuzzy kNN improves the fuzzy kNN algorithm by modifying the distance measure and introducing the weight for each feature.

In this study, we combine the three new indexes and the weighted fuzzy kNN algorithm to type the rocks. The process is as follows: let $XX = \{x_1, x_2, x_3, \cdots, x_n\}$, $YY = \{y_1, y_2, y_3, \cdots, y_m\}$ and $L = \{l_1, l_2, \cdots, l_c\}$ to be the set of the training points, test points and class labels, respectively. Obviously, XX, YY $\subseteq$ X, where X is a set of d-dimensional real-valued points. That is $x_i = (s_1, s_2, \cdots, s_d)$. In this study, d = 3. Each training point has three characteristic parameters (three rock typing indexes). For the training set, the class label for each training point x_i is known. While for $y_j \in YY$, its class label should be predicted. For the class label l_r, the number of training data points in it is assumed to be nn_r. Let the distance between two points be defined as $\delta(x_i, x_j)$.

For the training set XX, we use a matrix $U = [u_{ir}]_{n\times c}$ to store the membership u_{ir}, where u_{ir} is the probability that the training point x_i belongs to the class l_r, and $\sum_{r=1}^{c} u_r = 1$. Given a training set XX, there are many ways to calculate U, among which we use the method proposed by Keller et al. (1985), and describe it in expression

$$u_{ir} = \begin{cases} 0.49\left(\frac{n_r}{\nu}\right) & if\ c_L(x_i) \neq l_r \\ 0.51 + 0.49\left(\frac{n_r}{\nu}\right) & otherwise \end{cases} \tag{12}$$

Where n_r is the number of the training points having a class label l_r, ν is an integer $\nu \geq 1$. For a test point $y_j \in YY$. The fuzzy kNN returns a set $M(y_j) = \{\mu_1(y_j), \mu_2(y_j), \cdots, \mu_c(y_j)\}$ and $\mu_r(y_j)$ is the probability that y_j belongs to the rth class, given as:

$$\mu_r(y_j) = \frac{\sum_{x_i \in \Omega_k(P,\ y_j)} u_{ir}\delta_w(y_j,\ x_i)^{\frac{2}{1-m}}}{\sum_{x_i \in \Omega_k(P,\ y_j)} \delta_w(y_j,\ x_i)^{\frac{2}{1-m}}} \tag{13}$$

where m is a performance controlling parameter, and m > 1. Evidently, the higher the value of m the more the neighbors will be weighted equally irrespective of their distances from y_j.

Different from the kNN and the fuzzy kNN algorithms, the class-based feature weighted Euclidean distance $\delta_w(x_i, y_j)$ is used. This distance measure can be expressed as:

$$\delta_w(x_i, y_j) = \left(\sum_{f=1}^{d} w_{jf}\left(x_i^f - y_j^f\right)^2\right)^{\frac{1}{2}} \tag{14}$$

where w_{jf} is the weight for the f th dimension (the f th characteristic index) when the training point x_i belongs to l_r. Therefore, $W = [w_{rf}]_{c\times d}$

The weight for the f th rock typing indexe (f = 1, 2, 3) is calculated based on the training set. First, we should calculate the dispersion of each characteristic index for each class. The dispersion (denoted by θ) is calculated as follows:

$$\theta_r^f = \sqrt{\sum_{t=1}^{nn_r} \frac{s_{rt}^f}{\sum_{r=1}^{c} \bar{s}_r^f}}, \quad \bar{s}_r^f = \frac{\sum_{t=1}^{nn_r} s_{rt}^f}{nn_r} \tag{15}$$

where θ_r^f is the dispersion of the f th characteristic index, $\bar{s}_r^f$ is the average value the f th characteristic index for the class label l_r.

Then the weight for the f th rock typing indexes (f = 1, 2, 3) can be calculated as follows

$$w_{rf} = \frac{\theta_r^f}{\sum_{f=1}^{d} \theta_r^f} \tag{16}$$

Based on the weighted fuzzy kNN, each rock typing index proposed in this paper can be weighted for each class during typing rocks, which can improve the rock typing calculation accuracy and speed.

3. Results and discussion

In this section we will use the three new rock typing indexes and the weighted fuzzy kNN algorithm to type the tight sandstone.

3.1. The generation tight sandstone dataset in Ordas Basin

An ideal database to evaluate the proposed rock typing indexes would be one that includes the diversity information (such as pore and throat radius, pore and throat shape, connectivity, mineral distribution) of the tight sandstones in the research area. In this study, the research area is the Upper Triassic Yanchang Formation, Ordos Basin, NW China. Moreover, water-oil primary drainage capillary pressure, strongly dependent on pore geometry and microstructural characteristics, are integrated in the dataset and analyzed to validate the petrophysical rock typing indexes.

The procedure for constructing a dataset for tight sandstones in the research area is as follows. Fifty typical samples of actual tight sandstone in the Upper Triassic Yanchang Formation of Ordos Basin are analyzed to observe the trends and frequency of the petrophysical properties. Their porosity and permeability are measured by helium porosimetry and pulse-decay permeability measurement. Fig. 10 illustrates the probability density function (PDF) of the porosity and permeability of the samples. It can be seen that the porosity of most samples is below 10%, and the average porosity is 8.7%. The average value of

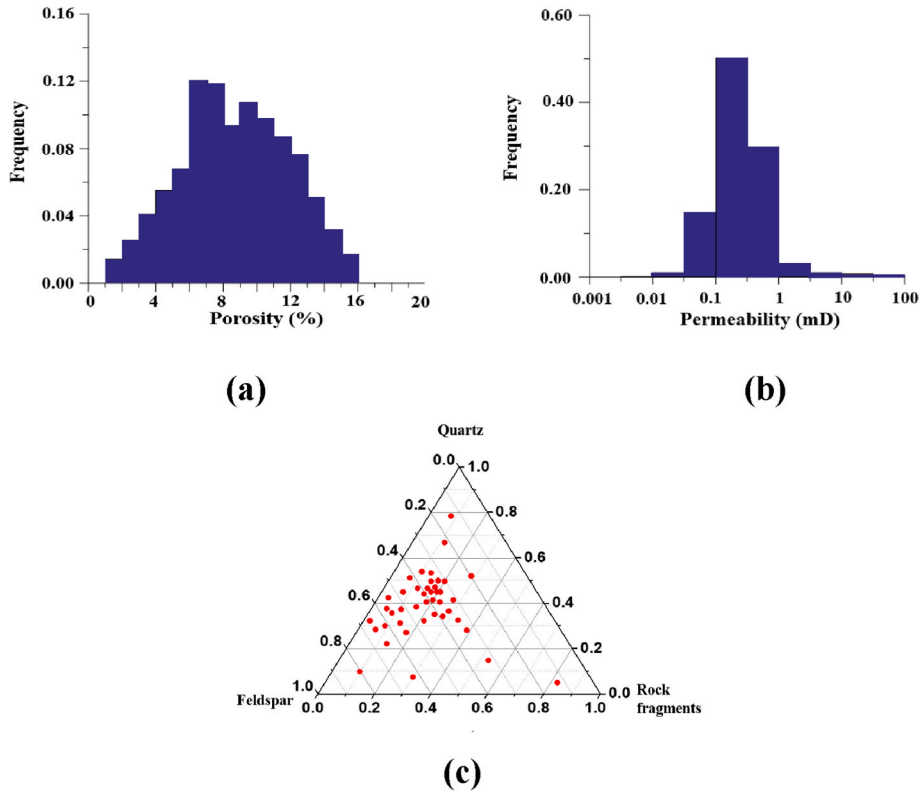

Fig. 10. The distribution of porosity (a), permeability (b) and mineral(c) of tight sandstones in Upper Triassic Yanchang Formation of Ordos Basin.

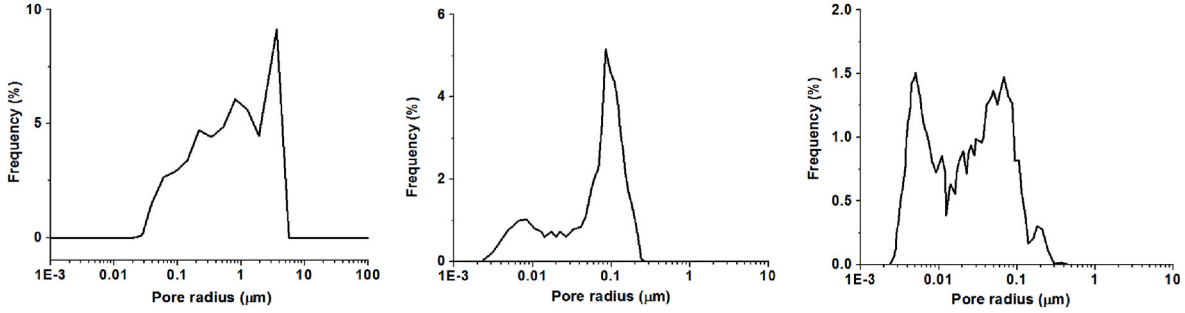

Fig. 11. The typical pore-size distribution of tight sandstone in Ordos Basin.

permeability is 0.24mD, and the tight sandstone in the research area has low porosity and permeability. In addition, the mineral compositions for the samples are also investigated by X-ray Powder Diffraction, and the results are shown in Fig. 10(c). Moreover, high-pressure mercury injection is employed to study the pore structure of some tight sandstones, and some typical results are given in Fig. 11. The tight sandstone can be classified into two types, one is mainly nanometer pores, and the other is mainly micron pore. The peaks of the pore radius are 10 nm, 100 nm and 2μm. The process of constructing the dataset is shown in Fig. 12. We have proved that when the 2D random pore network is large enough, it can represent the heterogeneity of the pore and contact angle in the 3D samples (see Appendix). Thus during constructing a dataset for tight sandstones, the 2D RES random pore networks are used to represent the characteristics of tight sandstone samples. To generate a more realistic and representative 2D pore network, we use the distribution of porosity, permeability, and mineral in Fig. 10 and the pore-size distribution in Fig. 11 as the constrained condition. The elements (pore and throat) of the pore network are assigned different shape factors, such as circular, square and triangular shape (Afsharpoor and Javadpour, 2016). Moreover, the diversity of the tortuosity of pore structure is also considered, as shown in Fig. 12. All the procedures mentioned above can ensure that the constructed pore network can represent the actual tight sandstone. In the second step, the properties of two-phase fluid flow are considered during calculating the capillary pressure based on the quasi-static pore network model and the pore network generated in the first step. Moreover, the diversity of the contact angle distribution, the wettability index, and the interfacial tension are all involved in the dataset, as shown in Fig. 12. Finally, we can obtain that the dataset which has both the petrophysical characteristics of the tight sandstones and the fluid flow properties. Finally, 5000 groups of data are generated and we will use them to examine the new indexes proposed in the above section.

3.2. Validation

We randomly choose 4500 samples from the dataset and train the weighted fuzzy kNN algorithm to obtain the weight for each rock typing index in each type of tight sandstone based on the methodology in Section 2. Then 500 samples are used to test the accuracy of the prediction results.

From the training set, we can determine the weight of each rock

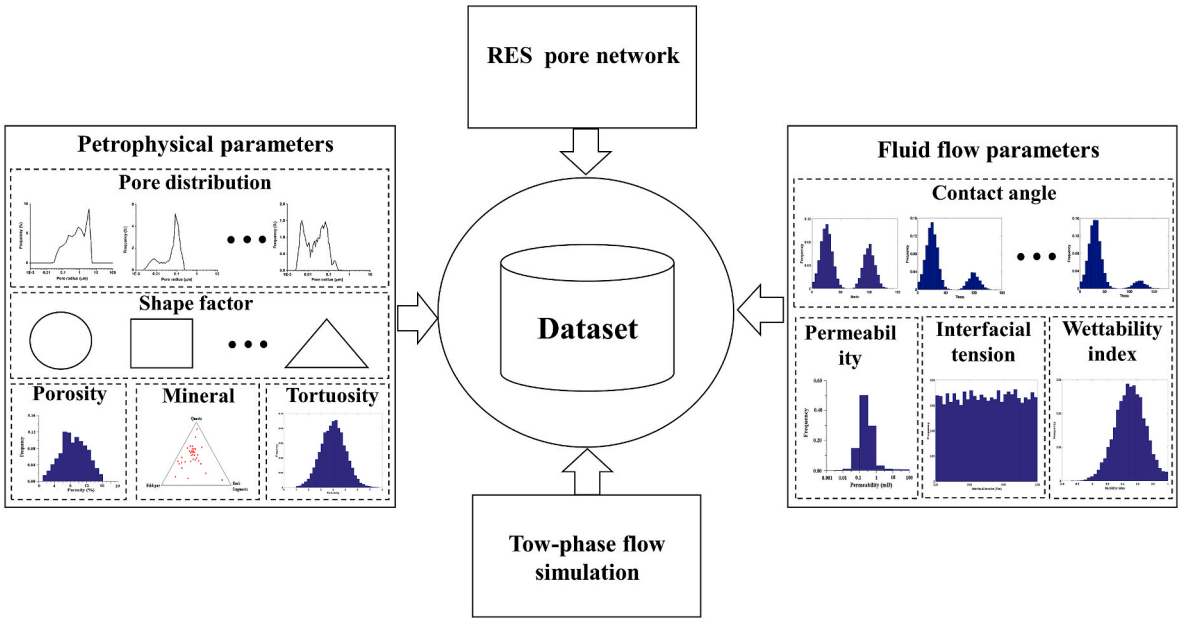

Fig. 12. The schematic diagram for constructing the dataset of tight sandstone.

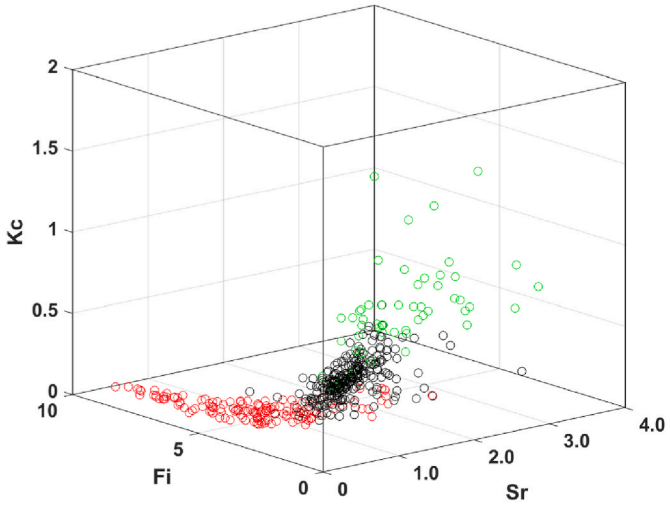

Fig. 13. The new indexes of each type tight sandstone for the test data.

typing index in each tight sandstone type through the weighted fuzzy kNN algorithm. Then based on these weights, we can get the classification results of the 500 samples in the test set, as shown in Fig. 13. It can be seen that the differences between the indexes of each type of rock are quite large. To further verify the accuracy of the classification results, we give the pore composition and the oil-water two-phase capillary pressure curves for samples in each type of rock, as shown in Fig. 14. It can be seen from the figure that the first type of rock sample is dominated by pores with a radius smaller than R_{Kc}, and the oil-water capillary pressure is larger than that of the other two types. The second type of rock sample is dominated by pores with a radius greater than R_{Kc} and less than R_{Sr}, and the oil-water capillary pressure is smaller than that of the first type. The third type of rock sample is dominated by pores with a radius greater than R_{Sr}, and the oil-water capillary pressure is the smallest. The oil-water capillary pressure curves of the three types have obvious differences in shape and value. The relative error of the test

Table 2
The comparison of relative errors for the rock typing method proposed in our paper, FZI, the kNN method.

	Our method	FZI	r35	The kNN method
relative error	0.05	0.28	0.31	0.13

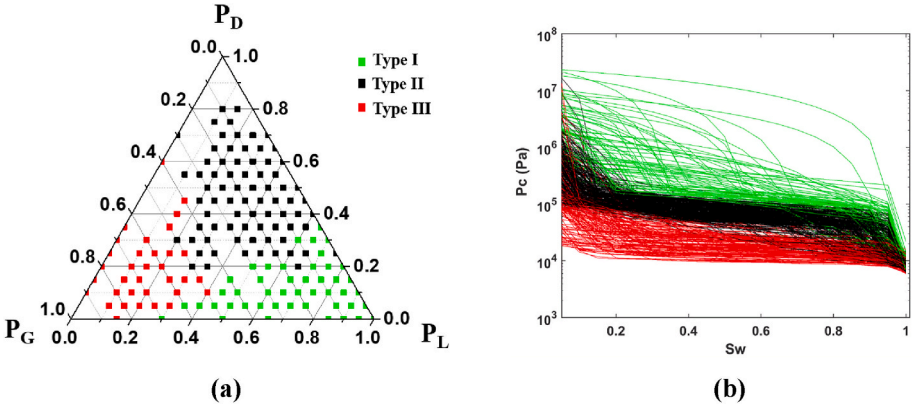

Fig. 14. The pore composition (a) and the oil-water capillary pressure curves (b) for each type tight sandstone for the test data.

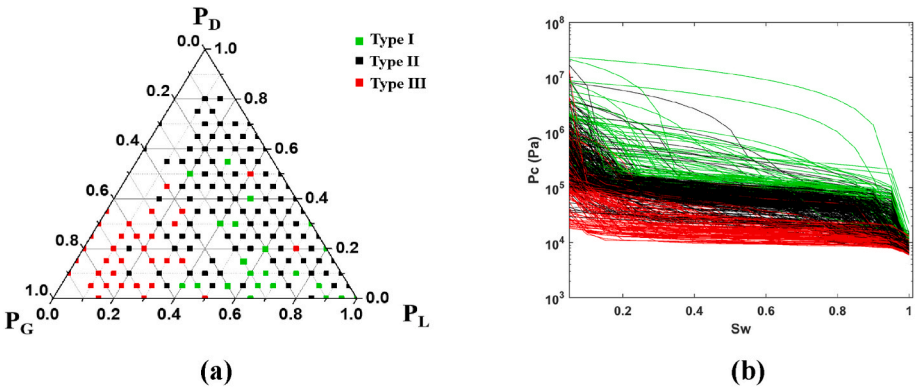

Fig. 15. The pore composition (a) and the oil-water capillary pressure curves (b) for each type tight sandstone obtained by FZI.

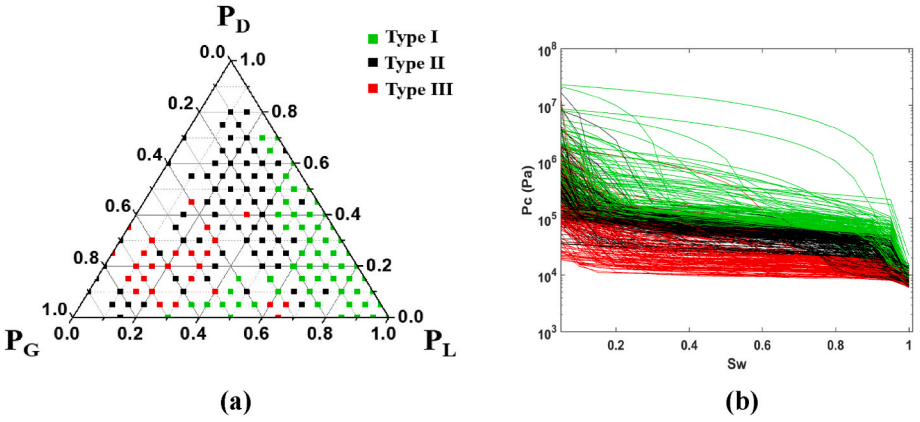

Fig. 16. The pore composition (a) and the oil-water capillary pressure curves (b) for each type tight sandstone obtained by r35.

results is listed in Table 2. We can find that it is less than 10%. The results validate the proposed typing indexes and the weighted fuzzy kNN algorithm.

Moreover, we compare our method with the conventional indexes (FZI and r35). Figs. 15 and 16 display the typing results of the test data by FZI and r35. It can be seen from the figures that there is a serious overlap between different types of pore composition and oil-water capillary pressure curves. The results demonstrate that the classification of some samples is not very good. By comparing Figs. 14, Fig. 15, and Fig. 16, we can obtain that the method proposed in our paper has better performance in the identification of the flow and pore structure characteristics of different types of tight sandstones.

To further examine the performance of the weighted fuzzy kNN algorithm, we compare it with the kNN method. That is considering and without considering the weight difference between different indexes. Fig. 17 plots the typing results of the test data by the kNN method. Inspecting Fig. 16, we can find that there is also some overlap between different types of pore composition and oil-water capillary pressure curves. Similar to FZI and r35, some samples have been assigned incorrect types. Then the relative errors of the test results for our method, FZI,r35, and kNN method are compared in Table 2. It can be concluded from Table 2 that the method proposed in our paper has the best performance in identifying the flow and pore structure characteristics for different types of tight sandstones.

Finally, 30 highly heterogeneous tight sandstone samples from the Upper Triassic Yanchang Formation, Ordos Basin have been used to

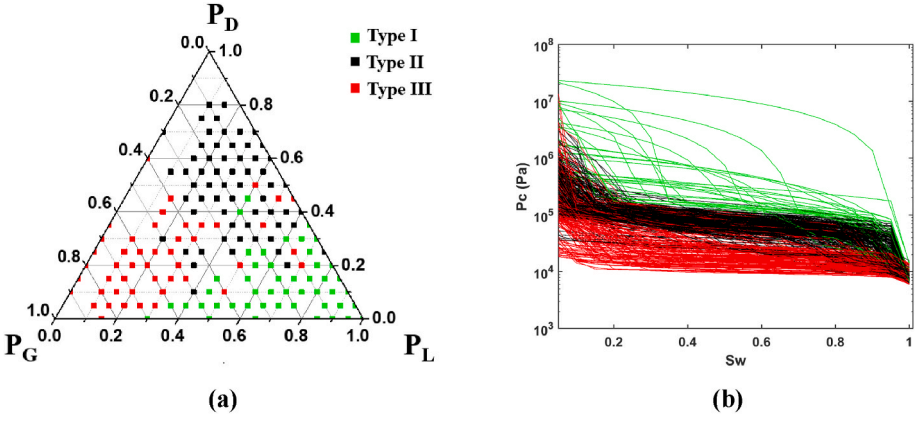

Fig. 17. The pore composition (a) and the oil-water capillary pressure curves (b) for each type tight sandstone obtained by the kNN method.

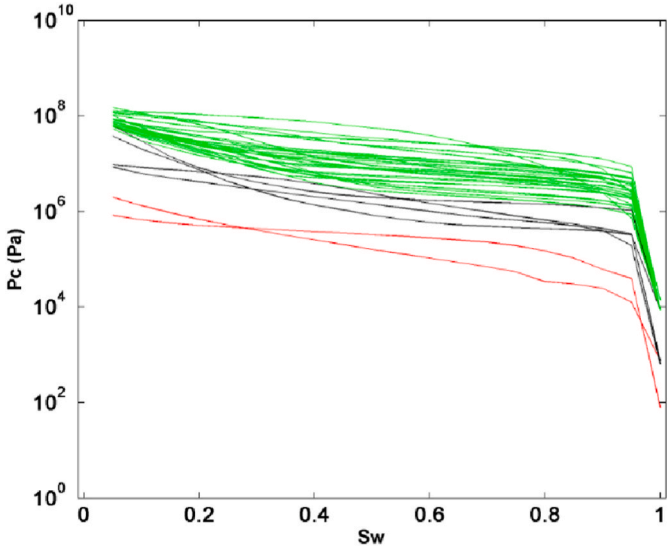

Fig. 18. The mercury injection capillary pressure (MICP) curves for each type of tight sandstone.

further validate our method. It should be pointed out that these samples are not included in the above dataset and they have a quite different mineral composition, pore structure, and permeability. After analyzing the samples by the proposed method in this paper, we can finally obtain that two samples belong to Type III, four samples belong to Type II and other 24 samples belong to Type I. Then the mercury injection capillary pressure (MICP) curves of the 30 samples are measured by experiment, as shown in Fig. 18. Fig. 18 demonstrates that there are relatively big differences in MICP curves between different types of rocks. The results once again prove that the new indexes and weighted fuzzy kNN algorithm have good typing performance for tight sandstone.

4. Conclusions

In this study, three new rock typing indexes have been proposed and then combined with the weighted fuzzy kNN algorithm to type tight sandstones. After analyzing the results, some important conclusions are summarized as follows:

1. The Darcy index, the gas non-Darcy index, and the liquid non-Darcy index have been proposed to type the tight sandstone. Moreover, based on the analysis of these indexes, the limit pore radius for gas non-Darcy and liquid non-Darcy flow have been determined. The pores can be divided into three parts: the gas non-Darcy flow part, the liquid non-Darcy flow part, and the -Darcy flow part. The results show that these three indexes can describe the flow characteristics and the pore composition of the tight sandstone.
2. The three new indexes describe different flow characteristics in tight sandstone and play different roles in typing the rocks. Their weights for each type of tight sandstone can be determined by the weighted fuzzy kNN algorithm. The final rock typing result shows that considering the weight difference between different indexes is more accurate than not considering the weight difference.
3. The dataset for tight sandstone in Upper Triassic Yanchang Formation, Ordos Basin, NW China has been constructed to test our method. The typing results have been compared with the conventional index FZI and r35. It can be obtained that tight sandstones of the same type have similar flow characteristics and pore composition, and the accuracy of our method is much better than the conventional indexes. In addition, 30 tight sandstone samples from the research area have been also used to evaluate our method. All the results have proved that the proposed new rock typing indexes and weighted fuzzy kNN algorithm can type the tight sandstone very well, and they can play a significant role in permeability prediction, reservoir modeling, and simulation.

It should also be emphasized that the rock typing indexes can be also used for reservoir drilling, production, injection, reservoir studies and simulation purposes. Moreover, from the discussion in the study, we can deduce that the pore structure and flow properties of each type of tight sandstone are quite different from each other. The oil-water primary drainage capillary pressure curves of the same type have relatively similar characteristics. Based on the typing results, we can further predict the water-oil primary drainage capillary curves by using a neural network, which will be discussed in another paper.

Author statement

Lili Ji: Methodology, Software, Writing – original draft, Mian Lin: Supervision, Conceptualization, Reviewing, Wenbin Jiang: Software, Data curation, Formal analysis. Gaohui Cao: Visualization, Investigation, Zhipeng Xu: Software, Validation. Fang Hao: Supervision, Reviewing and Editing.

Declaration of competing interest

The authors declare that they have no known competing financial interests or personal relationships that could have appeared to influence the work reported in this paper.

Acknowledgements

This work is supported by the National Natural Science Foundation of China (Grant No. 42030808, 41872163 and 41690132), the Strategic Priority Research Program of the Chinese Academy of Sciences (Grant No. XDA14010304).

Appendix. The representative element surface (RES) of the 2D random network

In this paper, the 2D random pore network is used to construct the tight sandstone dataset for typing the rocks. Thus in the following we will prove that the 2D random pore network that is large enough can represent the 3D digital core of the tight sandstones samples. In other words, the 2D random pore network that is large enough will have similar properties (such as porosity, absolute permeability, capillary pressure curves, etc.) to the 3D digital core.

The typical sandstone (Berea sandstone) and tight sandstone have been used to investigate under what condition the 2D random pore network can represent the 3D digital core. The 3D digital core of Berea sandstone with the size of 400*400*400 pixels is shown in Fig. A1a, and its resolution is

5.345μm. The pore network of Berea sandstone is extracted by the pore network extraction algorithm (the axis & ball algorithm) developed by Yi (Yi et al., 2017), and the pore-size distribution is shown in Fig.A2a. It can be seen that the pore of Berea sandstone is homogeneous. The 3D digital core of a tight sandstone sample is shown in Fig.A1b and its corresponding pore-size distribution is also shown in Fig. A2b. It can be seen that the pore of tight sandstone is much more inhomogeneous than that of Berea sandstone. Then with the pore size distribution in Fig.A2 as the constraint condition, the 2D random pore network of the two kind of stones are constructed, as shown in Fig.A3.

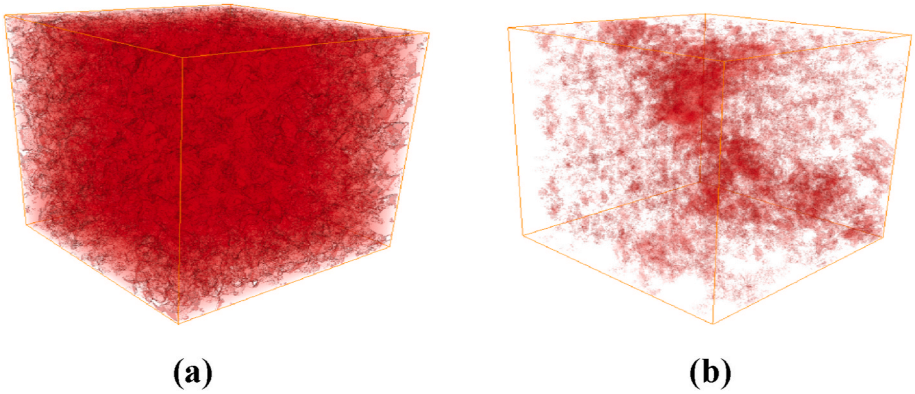

Fig. A1. the digital core of the Berea sandstone (a) and the tight sandstone (b).

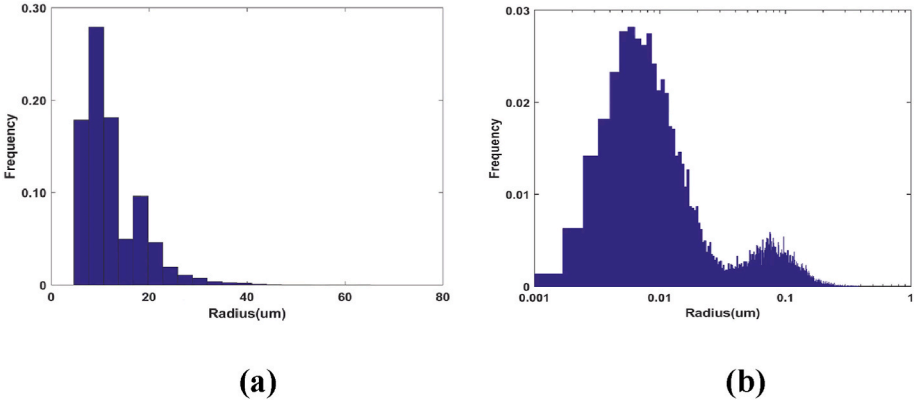

Fig. A2. The pore size distribution of Berea sandstone (a) and the tight sandstone (b).

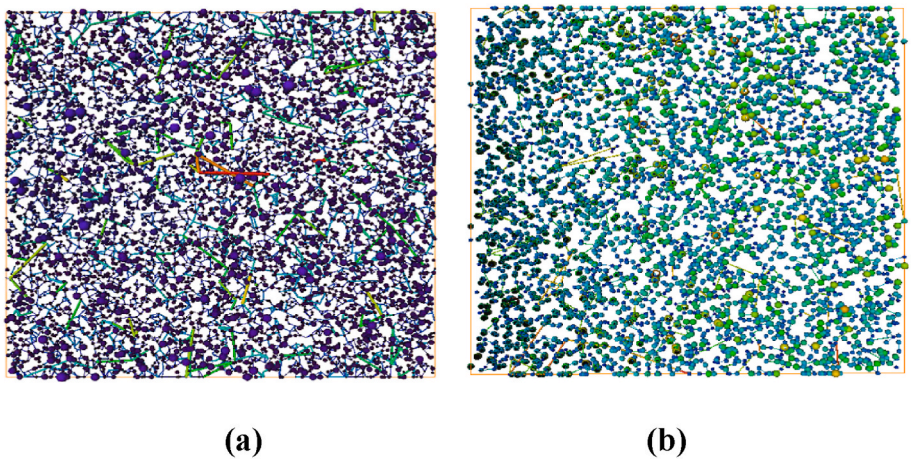

Fig. A3. The 2D random pore network of Berea sandstone (a) and the tight sandstone (b).

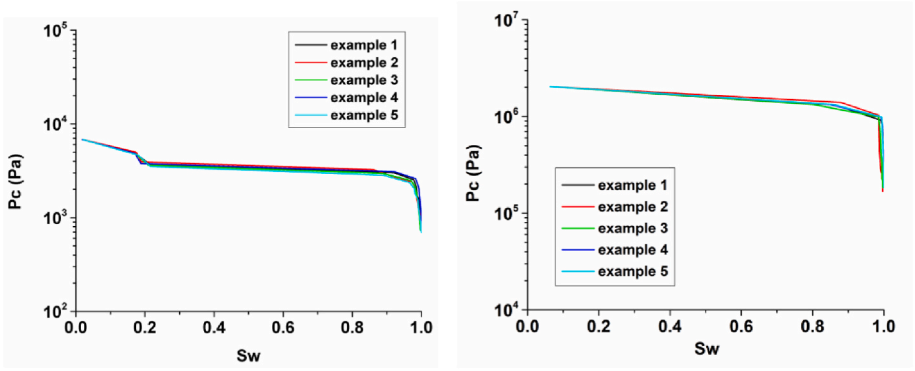

Fig. A4. The capillary pressure curves for five different 2D RES random pore networks of Berea sandstone (a) and tight sandstone (b).

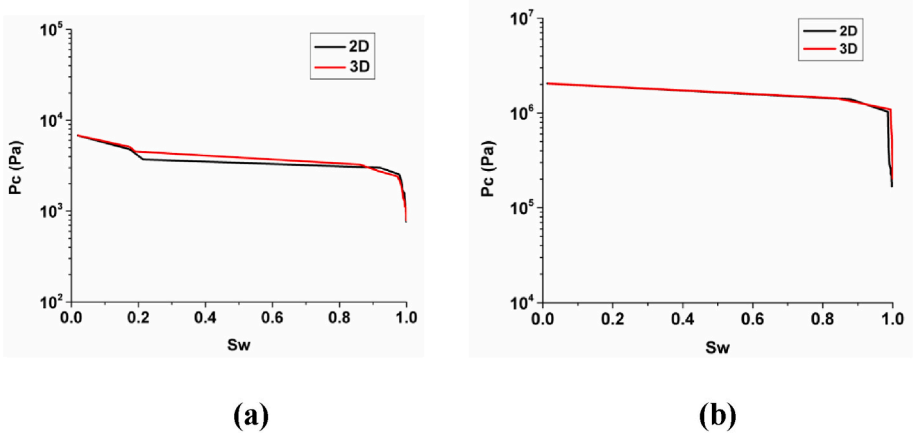

Fig. A5. The comparison of capillary pressure curves between the 2D RES random pore networks and the 3D digital core of Berea sandstone (a) and tight sandstone (b).

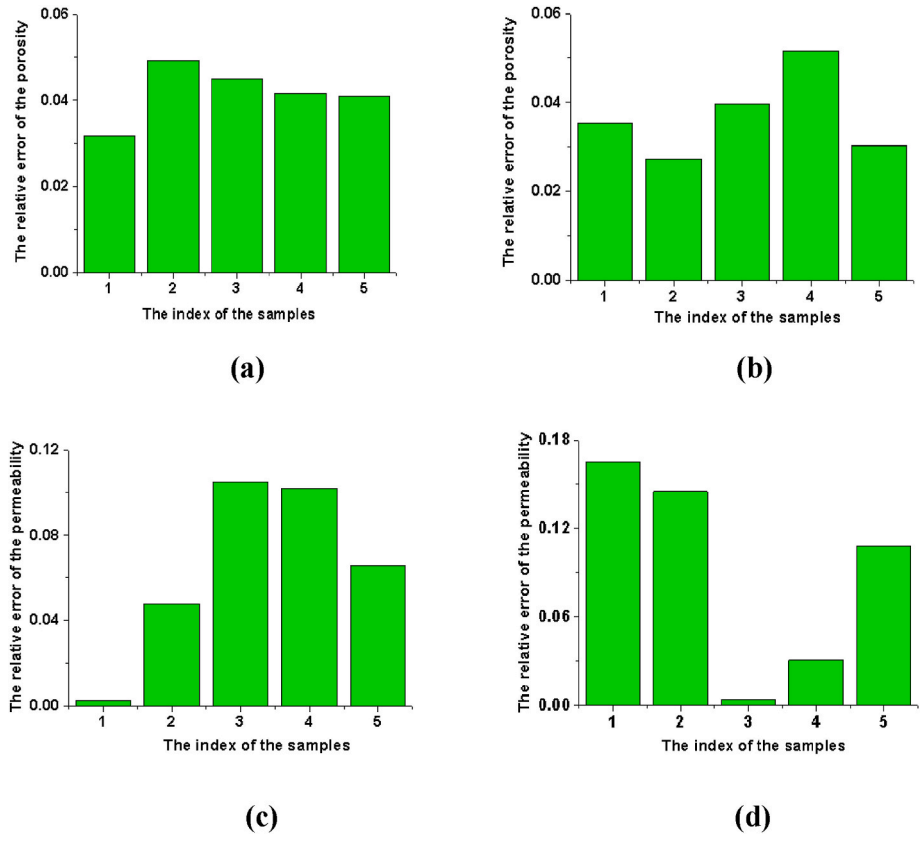

Fig. A6. The relative error of the porosity between the 2D RES random pore networks and the 3D digital core for Berea sandstone (a) and tight sandstone (b); the relative error of the absolute permeability between the 2D RES random pore networks and the 3D digital core for Berea sandstone (c) and tight sandstone (d).

In this paper RES (representative element surface) is defined as the surface that is sufficient to involve the heterogeneity of the pore and contact angle in the 3D tight sandstone samples. First of all, we define the ratio of the side length of the 2D pore network and the 3D digital core of the core samples as Dr, which will help us to study the relation between the 2D pore network and the 3D digital core. Furthermore, to evaluate the heterogeneity of the pore and contact angle, we define the ration (signed by V) between variance and mean of the pore and contact angle as Vp and Vc. In this section we will examine the heterogeneity of the pore and contact angle respectively.

First, we assume that all the elements (pores and throat) in the Berea and the tight sandstone have the same water-oil contact angle which is 30°. Then we study the influence of the heterogeneity of the pore on the size of the RES random pore network. We enlarge the size of the 2D pore network until it reaches RES. We have found that when the number of pores in 2D pore network of Berea sandstone is bigger than 5000 and Vr is 4.87, the capillary pressure curves for oil-water two-phase flow of the five different 2D random pore networks which follow the same pore size distribution are almost the same, as shown in Fig.A4a. At the same time there are little difference in the capillary pressure curves, the porosity and absolute permeability between the 2D pore network and 3D digital core, as shown in Fig.A5a, Fig.A6a and Fig.A6c. Furthermore, we have found that when the number of pore is more than 10000 and Vr is 6.45, the 2D pore network for tight sandstone reach RES, as shown in Fig. A4b. Also the capillary pressure curves, the porosity and absolute permeability between the 2D pore network and 3D digital core are almost the same, as shown in Fig. A5b, Fig.A6b and Fig.A6d.

Second, we further investigate the effect of the heterogeneity of contact angle on the size of the RES pore network. Fig. A7 plot the distribution of the contact angle in the Berea and the tight sandstone. From calculation, we obtain that Vc of the Berea and tight sandstone are 0.65 and 0.76. Then during generating the 2D random pore network and simulating the oil-water flow, we assign each element (pore and throat) the contact angle with the function in Fig. A7 as constrain condition. Like the discussion in the above paragraph, we enlarge the size of the 2D pore network until it reaches RES. We finally find that when the number of pores in 2D pore network of Berea sandstone is bigger than 10000 and Vr is 7.13, the capillary pressure curves for oil-water two-phase flow of the five different 2D random pore networks which follow the same pore size and contact angle distribution are almost the same, as shown in Fig. A8a. Inspecting Fig. A9a, we can also deduce that the capillary pressure curves of the 2D network has a good agreement with that of the 3D digital core. The other network element property, porosity, is also estimated, as shown in Fig.A10a. The relative error of the porosity between the 2D pore network and the 3D digital is smaller than 10%. For the tight sandstone, when the number of pores in 2D pore network is bigger than 15000 and Vr is 7.13, the capillary pressure curves for oil-water two-phase flow of the different 2D random pore networks are almost the same, as shown in Fig. A8b. Furthermore, the capillary pressure curves, the porosity and absolute permeability of the 2D pore network agree very well with that of the 3Ddigital core. Therefore we can derive that the 2D RES random pore network can represent the 3D digital core of tight sandstone.

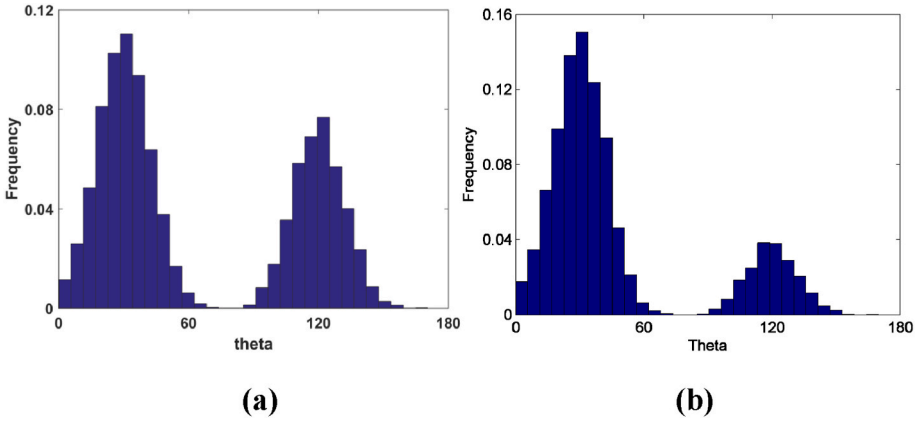

Fig. A7. The contact angle distribution of Berea sandstone (a) and the tight sandstone (b).

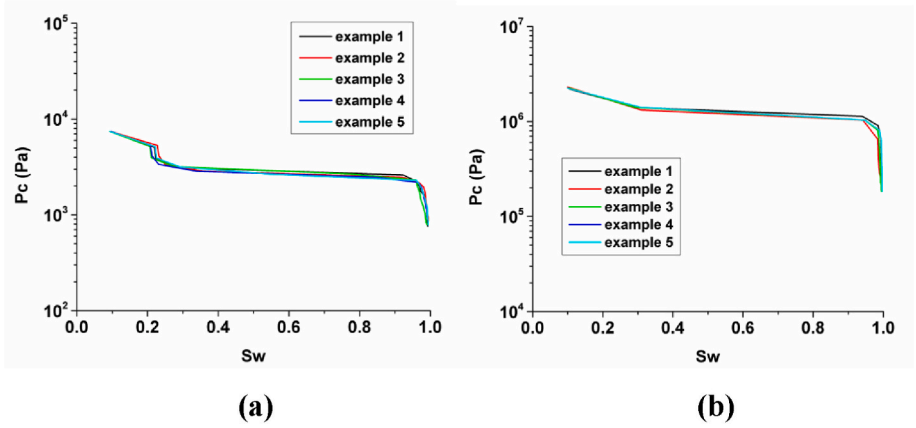

Fig. A8. The capillary pressure curves for five different 2D RES random pore networks for Berea sandstone (a) and the tight sandstone (b).

Finally, we list the relation between the heterogeneity of the pore, contact angle and the size of RES of the samples in Table A1. It can be seen that the size of the RES pore network which can represent the 3D core depend on the heterogeneity of pore and contact angle (Carman, 1937; Chen and Zhou, 2017). Especially, if we consider the heterogeneity of contact angle, it needs larger size of the RES pore network than only considering the heterogeneity of pore. Moreover, as the heterogeneity of pore and contact angle increase, Vr and Vc increase.

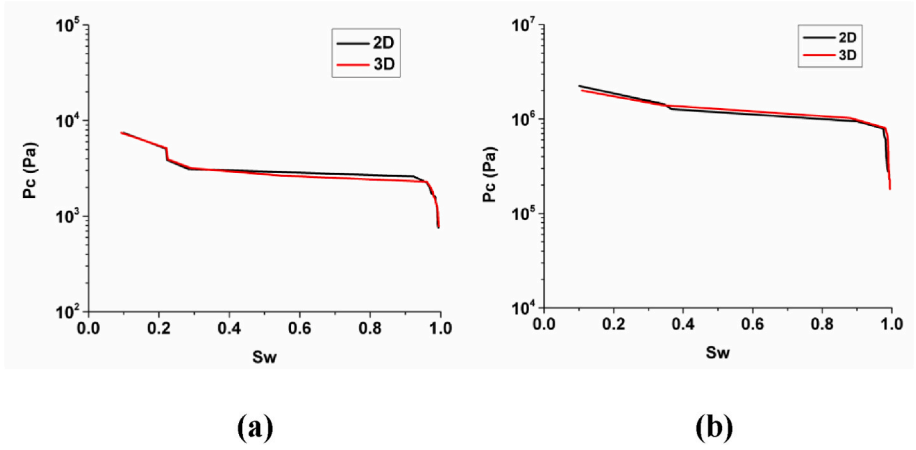

Fig. A9. The comparison of capillary pressure curves between the 2D RES random pore networks and the 3D digital core of Berea sandstone (a) and the tight sandstone (b).

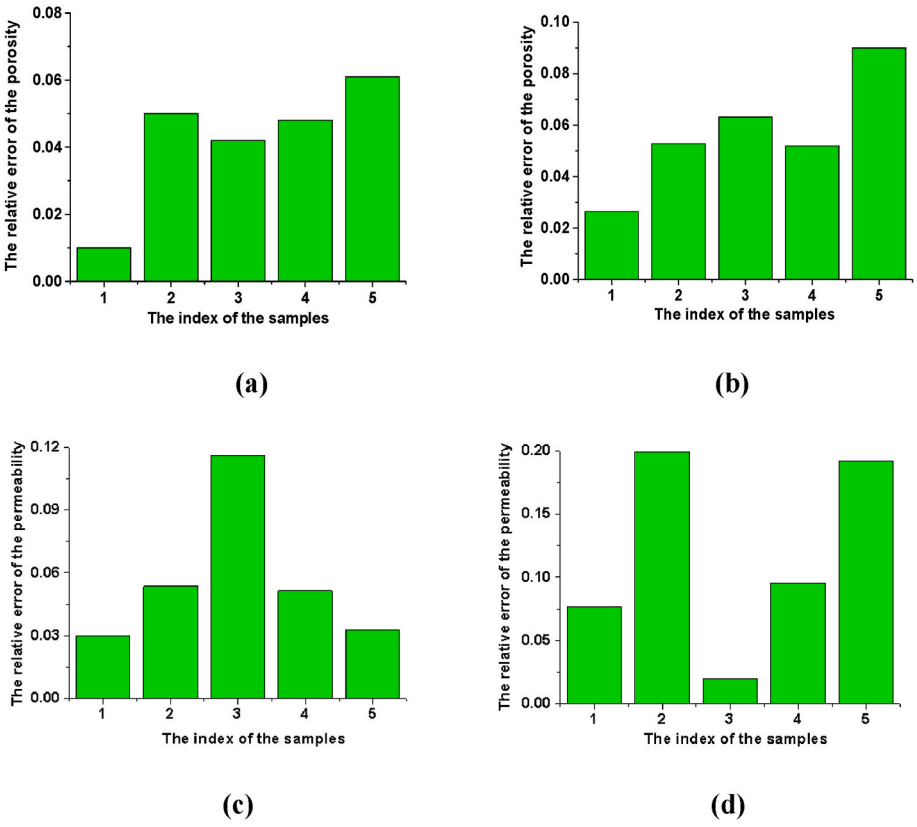

Fig. A10. The relative error of the porosity between the 2D RES random pore networks and the 3D digital core of Berea sandstone (a) and tight sandstone (b); the relative error of the absolute permeability between the 2D RES random pore networks and the 3D digital core for Berea sandstone (c) and tight sandstone (d);

Table A1
The relation between the heterogeneity of the pore, contact angle and the size of RES pore network of the samples

	The heterogeneity of the pore		The heterogeneity of contact angle	
	Vp	Dr	Vc	Dr
Berea	**0.52**	**4.87**	**0.65**	**7.13**
Tight sandstone	**0.96**	**6.45**	**0.78**	**9.60**

To obtain more general result, we further examine three typical tight sandstone in Ordos Basin, NW China with the pore-size distribution in Fig. 11. The heterogeneity of the pores for the three samples are calculated, and they are 0.63, 0.76 and 0.87 respectively. Then the RES random pore network for the samples are constructed with the pore-size distribution as constrain condition. The ratios of the side length of the 2D pore network and the 3D digital core of three samples are 5.116, 5.33 and 6.32. Then to investigate the relationship between the heterogeneity of the pore and the size of RES, Vp and Dr for the three tight sandstones and the two samples in Fig.A1 are all given in Fig. A11. It can be seen that Dr increases approximately linearly with Vp.

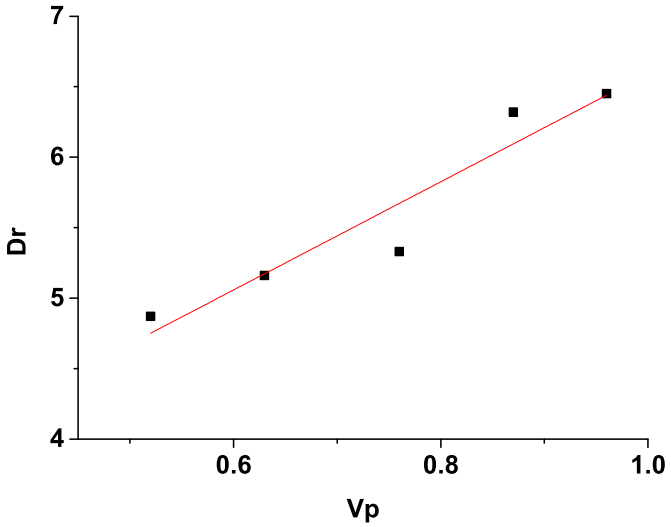

Fig. A11. The relationship between Vp and Dr.

In sum, we can deduce that for any 3D tight sandstone, we can find an RES pore network that is big enough to represent the heterogeneity of the pore and contact angle of the actual 3D samples. Thus in this paper, the 2D RES pore network is used to study the two-phase flow in tight sandstone.

References

Abbaszadeh, M., Fujii, H., Fujimoto, F., 1996. Permeability prediction by hydraulic flow units -theory and applications. SPE Form. Eval. 11, 263–271.

Amaefule, J.O., Altunbay, M., Tiab, D., et al., 1993. Enhanced reservoir description: using core and log data to identify hydraulic (flow) units and predict permeability in uncored intervals/wells. In: Presented at the SPE Annual Technical Conference and Exhibition. Houston, 3–6 October. SPE-26436-MS.

Audry, M.C., Poednoir, P., Joseph, P., et al., 2010. Amplification of electroosmotic flows by wall slippage: direct measurements on OTS surface. Faraday Discuss 146, 113–124.

Berg, R.R., 1970. Method for determining permeability from reservoir rock properties. Trans. Gulf Coast Assoc. Geol. Soc. 20, 303–317.

Carman, P.C., 1937. Fluid flow through granular beds. Trans. Inst. Chem. Eng. 15, 150–166.

Chen, X., Yao, G., 2017. An improved model for permeability estimation in low permeable porous media based on fractal geometry and modified Hagen-Poiseuille flow. Fuel 210, 748–757.

Chen, X., Zhou, Y., 2017. Applications of digital core analysis and hydraulic flow units in petrophysical characterization. Adv. Geo-energy Res. 1 (1), 18–30.

Coppens, M.O., 1999. The effect of fractal surface roughness on diffusion and reaction in porous catalysts from fundamentals to practical applications. Catal. Today 53 (2), 225–243.

Coppens, M.O., Dammers, A.J., 2006. Effects of heterogeneity on diffusion in anopores from inorganic materials to protein crystals and ion channels. Fluid Phase Equil. 246 (1–2), 308–316.

Cottin, B.C., Cross, B., Steinberger, A., et al., 2005. Boundary slip on smooth hydrophobic surfaces: intrinsic effects and possible artifacts. Phys. Rev. Lett. 94, 056102.

Ferreira, F.C., Booth, R., Oliveira, R., Carneiro, G., Bize-Forest, N., Wahanik, H., 2015. New rock-typing index based on hydraulic and electric tortuosity data for multi-scale dynamic characterization of complex carbonate reservoirs. In: SPE-175014-MS, SPE Annual Technical Conference and Exhibition, pp. 28–30.

Hartmann, D.J., Coalson, E.B., 1990. Evaluation of the Morrow Sandstone in the Sorrento Field, Cheyenne Company. Rocky Mountain Association of Geologists, Colorado, pp. 91–100.

Jaya, I., Sudaryanto, A., Widarsono, B., 2005. Permeability prediction using pore throat and rock fabric: a model from Indonesian reservoirs. In: Presented at the SPE Asia Pacific Oil and Gas Conference and Exhibition. Jakarta, 5–7 April. SPE-93363-MS.

Jiang, W.B., Lin, M., Yi, Z.X., et al., 2017. Parameter determination using 3D FIB-SEM images for development of effective model of shale gas flow in nanoscale pore clusters. Transport Porous Media 117, 5–25.

Kolodzie Jr., S., 1980. Analysis of pore throat size and use of the waxman-smits equation to determine OOIP in spindle field, Colorado. In: Presented at the SPE Annual Technical Conference and Exhibition. Dallas, 21–24 September. SPE-9382-MS.

Leverett, M.C., 1941. Capillary pressure in porous solids. Trans., AIME 142, 341–358.

Li, X.F., Fan, P., Wu, Y., Huang, Q.D., 2019. Study on abandonment formation pressure of Sulige tight sandstone gas reservoirs. China Science Paper 14 (8), 932–936.

Li, C.X., Lin, M., Liu, J., et al., 2021. The probability of oil and water movement in tight sandstone: evaluation methodology and mechanism analysis. J. Petrol. Sci. Eng. 196, 107661.

Lucia, F.J., 1983. Petrophysical parameters estimated from visual descriptions of carbonate rocks: a field classification of carbonate pore space. J. Petrol. Technol. 35 (3), 629–637.

Martin, A.J., Solomon, S.T., Hartmann, D.J., 1997. Characterization of flow units in carbonate reservoirs. AAPG (Am. Assoc. Pet. Geol.) Bull. 18 (5), 734–759.

Mirzaei-Paiaman, A., Ostadhassan, M., Rezaee, R., Saboorian-Jooybari, H., Chen, Z., 2018. A new approach in petrophysical rock typing. J. Petrol. Sci. Eng. 166, 445–464.

Ngo, V.T., Lu, V.D., Nguyen, M.H., et al., 2015. A comparison of permeability prediction methods using core analysis data. In: Presented at the SPE Reservoir Characterization and Simulation Conference and Exhibition. Abu Dhabi, 14–16 September. SPE-175650-MS.

Nooruddin, H., Hossain, M., 2011. Modified Kozeny-Carmen correlation for enhanced hydraulic flow unit characterization. J. Petrol. Sci. Eng. 80, 107–115.

Oliveira, G.P., Roque, W.L., Araújo, E.A., Diniz, A.A.R., Simoes, T.A., Santos, M.D., 2016. ~Competitive placement of oil perforation zones in hydraulic flow units from centrality measures. J. Petrol. Sci. Eng. 147, 282–291.

Pittman, E.D., 1992. Relationship of porosity and permeability to various parameters derived from mercury injection-capillary pressure curves for sandstone. AAPG Bull. 76, 191–198.

Rafiei, Y., Motie, M., 2019. Improved reservoir characterization by employing hydraulic flow unit classifification in one of Iranian carbonate reservoirs. Adv. Geo-Energy Res. 3 (3), 277–286.

Rezaee, R., Saeedi, A., Clennell, B., 2012. Tight gas sands permeability estimation from mercury injection capillary pressure and nuclear magnetic resonance data. J. Petrol. Sci. Eng. 88 (89), 92–99.

Roque, W.L., Oliveira, G.P., Santos, M.D., Simoes, T.A., 2017. Production zone placements ~based on maximum closeness centrality as strategy for oil recovery. J. Petrol. Sci. Eng. 156, 430–441.

Saboorian-Jooybari, H., 2017. A structured mobility-based methodology for quantification of net-pay cutoff in petroleum reservoirs. SPE-183643-PA. SPE Reservoir Eval. Eng. 20 (2), 1–17.

Stolz, A., Graves, R.M., 2003. Sensitivity Study of Flow Unit Definition by Use of Reservoir Simulation, SPE Paper 84277. SPE Annual Technical Conference and Exhibition, Denver, 5-8 Oct.

Xu, Z.P., Lin, M., Jiang, W.B., Ji, L.L., Cao, G.H., 2021. Rapid multiscale pore network modeling for drainage in tight sandstone. J. Petrol. Sci. Eng. 204, 108682.